# Binding of the anticancer drug BI-2536 to human serum albumin. A spectroscopic and theoretical study

Jesús Fernández-Sainz [a], Pedro J. Pacheco-Liñán [a], José M. Granadino-Roldán [b], Iván Bravo [a], Andrés Garzón [a,*], Jaime Rubio-Martínez [c] and José Albaladejo [d]

[a] *Departamento de Química Física, Facultad de Farmacia, Universidad de Castilla-La Mancha, Paseo de los Estudiantes, s/n, 02071, Albacete, Spain*

[b]*Departamento de Química Física y Analítica, Facultad de Ciencias Experimentales, Universidad de Jaén, Campus "Las Lagunillas" s/n, 23071, Jaén, Spain*

[c] *Departament de Química Física, Universitat de Barcelona (UB) and the Institut de Recerca en Quimica Teorica i Computacional (IQTCUB), Martí iFranqués 1, 08028, Barcelona, Spain*

[d]*Departamento de Química Física, Facultad de Ciencias Químicas, Universidad de Castilla-La Mancha, Avenida Camilo José Cela, 10, 13071, Ciudad Real, Spain*

* *e-mail: andres.garzon@uclm.es*

## Abstract

BI-2536 is a potent Polo-like kinase inhibitor which induces apoptosis in diverse human cancer cell lines. The binding affinity of BI-2536 for human serum albumin (HSA) protein may define its pharmacokinetic and pharmacodynamic profile. We have studied the binding of BI-2536 to HSA by means of different spectroscopic techniques and docking calculations. We have experimentally observed that the affinity of BI-2536 for HSA is higher than that of other common HSA binding drugs. Therefore, it can be postulated that the drug dose should be increased to achieve a certain concentration of free drug in plasma, although BI-2536 could also reach tumour tissues by uptaking HSA/BI-2536 complex. Only a single binding site on HSA has been observed for BI-2536 which seems to correspond to the subdomain IIA pocket. The formation of the

HSA/BI-2536 complex is a spontaneous and entropy-driven process that does not cause a significant change of the secondary structure of the protein. Its endothermic character could be related to proton release. Thermodynamic analysis showed that the main protein - drug interactions are of the van der Waals type although the presence of amide and ether groups in BI-2536 could also allow H-bonding with some residues in the subdomain IIA pocket.

**Keywords:** BI-2536; human serum albumin; fluorescence quenching; drug-protein binding; ligand-protein docking

## 1. Introduction

BI-2536, a dihydropteridinone derivative, is a potent ATP-competitive Polo-like kinase 1 (PLK1) inhibitor which has already been studied in both preclinical and clinical phases (see Fig. 1) [1-5]. PLK1 belongs to a large family of conserved serine/threonine protein kinases and has been proposed as an attractive and novel anticancer drug target because of its key role in processes such as mitosis and cytokinesis [5,6]. Thus, overexpression of PLK1 is tightly associated with the development of cancer in humans as breast, colorectal, prostate and non-small cell lung cancer [5]. The biological activity of BI-2536 has been proved both *in vitro* and *in vivo* drawing great attention to its PLK1 inhibitory capacity in diverse cancer cells. Apart from inhibiting PLK1, BI-2536 also cross-inhibits other kinases such as PLK2 and PLK3, although less efficiently.

Human serum albumin (HSA) is the most abundant protein of blood plasma and binds a wide variety of drugs and endogenous ligands. It plays a vital role in physiological processes like the regulation of colloidal osmotic pressure and the transport of numerous endogenous compounds such as fatty acids, hormones, bile acids, amino acids, metals and toxic metabolites [7-9]. HSA can alter the pharmacokinetic and pharmacodynamic

properties of drugs, decrease their side effects, protect them against oxidation and improve targeting [9-11]. A certain degree of albumin-binding is required to solubilize some compounds that would otherwise aggregate and undergo a poor distribution. However, drugs with high affinity for HSA require higher doses to reach the effective concentration because only molecules in unbound form interact with therapeutic targets [11]. Hence, albumin-drug binding is an essential factor to determine the pharmacokinetics and pharmacological profile of drugs.

It has been reported that the altered organization of tumour vasculature results in vascular leakage and the accumulations of macromolecules (> 40 kDa), preferentially HSA, within the tumour interstitium [9,12-14]. Albumin is used by tumours as a source of energy and, therefore, when a HSA/drug complex is uptaken into a tumour, it is metabolized delivering the drug [14]. In this sense, important applications of plasma proteins on anticancer drug delivery have been reported [9,12-14]. For instance, Abraxane®, a paclitaxel-loaded in albumin nanoparticle, was approved for cancer therapy by the European Commission in 2008 [14]. The aim of this work is to study the association process of BI-2536 with HSA by means of steady state and time resolved fluorescence (SSF and TRF, respectively), UV-Vis absorption and Fourier transform infrared (FTIR) spectroscopies. HSA shows native fluorescence because of one tryptophan residue (TRP214) located in the subdomain IIA (also known as drug site 1, see Fig. 1) [9,11]. The intrinsic fluorescence of proteins due to tryptophan is highly sensible to its local environment. Changes in the emission spectra of tryptophan often occur in response to conformational transitions, subunit associations, substrate binding or denaturalization [15]. Fluorescence quenching is therefore a useful method to study binding processes between proteins and drugs. In order to get a deeper insight into the

interactions being established for the protein-ligand complex a biased docking protocol followed by a second scoring was also performed.

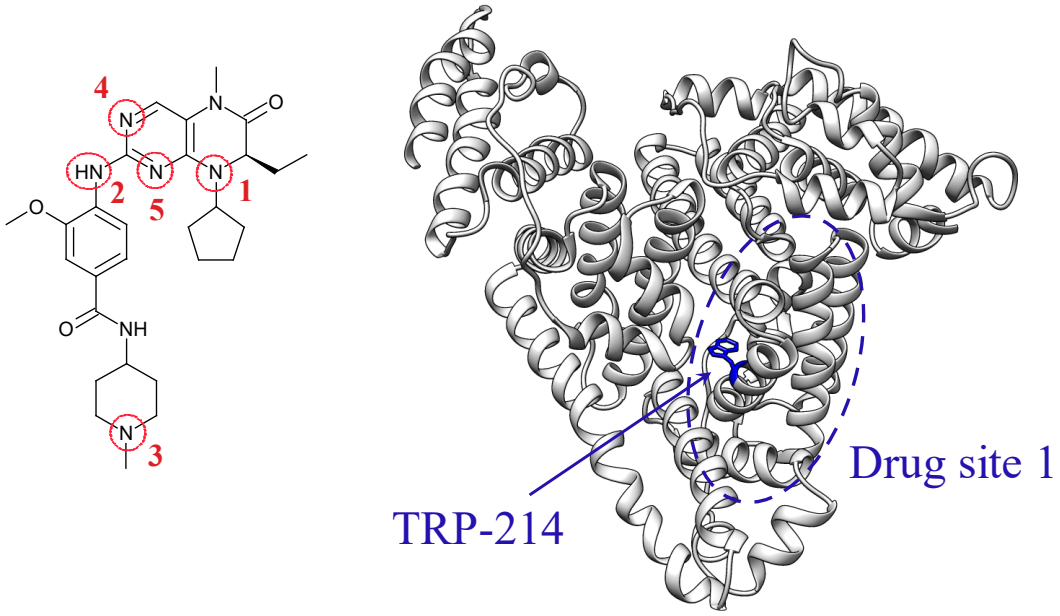


**Fig. 1.** Chemical formula of BI-2536 showing the protonation sites and X-ray structure of human serum albumin (pdb-entry 1AO6) [16].

## 2. Material and methods

### 2.1. Chemicals

BI-2536 (≥99.5%) was supplied by MedChem Express. HSA (≥99%; fatty acids and Globulin free), ibuprofen (> 98%) and warfarin (99.9%) were supplied by Sigma-Aldrich. The samples were dissolved in 0.02 M Tris-HCl buffer solutions at pH 7.4 containing 0.1 M NaCl. Bis-Tris (Sigma) and NaCl (Panreac) had a purity of no less than 99.0%. Water was purified in a Mili-RO System (Millipore).

### 2.2. Equipment and spectral measurements

The UV-Vis absorption spectra of BI-2536 were recorded using a Cary 100 (Varian) spectrophotometer in a 10 mm quartz cuvette, with a step of 1 nm and at room

temperature. Solutions of BI-2536 (10 μM) were prepared in different solvents. Small volumes of concentrated HCl and NaOH solutions were also added to the aqueous solutions of BI-2536 in order to collect its spectra at different pHs. Fluorescence spectra of the samples were recorded employing a FLS920 (Edinburgh Instruments) spectrofluorometer equipped with a time correlated single photon counting (TCSPC) detector. A Xe lamp of 450 W and a sub-nanosecond pulsed Light-Emitting Diode, EPLED-290 (Edinburgh Photonics) were employed as light sources at 291 nm to record the SSF and TRF spectra.

For HSA/BI-2536 binding experiments, working solutions of HSA (5 μM) were daily prepared in buffer solution and titrated in cuvette by successive addition of a BI-2536 solution (6.0 mM). The final concentration of BI-2536 in HSA solution varied from 0.0 to 50.0 μM (the [BI-2536]:[HSA] ratios were 0; 1; 2; 3; 5; 7; and 10). For SSF spectra, the excitation wavelength chosen was 295 nm to avoid the excitation of tyrosine and the emission fluorescence intensity was collected at 320 nm. Tryptophan fluorescence from HSA was corrected for the inner filter effect through

$$F_{corr} = F_{obs}\, 10^{(A_{exc}+A_{em})/2} \quad (1)$$

where $F_{corr}$ and $F_{obs}$ are the corrected and observed fluorescence intensities, and $A_{ex}$ and $A_{em}$ are the absorbance of the system at excitation and emission wavelengths (295 and 320 nm, respectively) [15]. The excitation and emission slits were fixed at 1 and 5 nm, respectively. The step and dwell time were 1 nm and 0.1 s, respectively. Temperature was controlled within 298 – 310 K by a temperature-controlled cuvette holder, TLC 50 (Quantum Northwest). Each experiment was repeated at least four times.

TRF emission was also collected at 320 nm. The fluorescence intensity decay, *I(t)*, was fitted to the following multiexponential function using an iterative least square fit method

$$I(t) = \sum_{i=1}^{n} \alpha_i \exp(-t/\tau_i) \quad (2)$$

where $\alpha_i$ and $\tau_i$ are the amplitude and lifetime for each *i*th term. The mean lifetime of the decay was then calculated as

$$\tau_m = \frac{\sum_{i=1}^{n} \alpha_i \tau_i^2}{\sum_{i=1}^{n} \alpha_i \tau_i} \quad (3)$$

FTIR measurements were carried out at room temperature using a 640-IR (Varian) spectrophotometer equipped with an attenuated total reflection (ATR) accessory. The spectra of HSA (1 mM), BI-2536 (1 mM) and HSA+BI-2536 (1 mM, molar ratio of 1:1) solutions were recorded with resolution of 4 $cm^{-1}$ and 64 scans. HSA+BI-2536 spectrum was corrected with the absorbance spectra of both the buffer solution and free BI-2536.

### 2.3. Analysis of fluorescence quenching measurements

Fluorescence quenching is generally described by the Stern-Volmer equation

$$F_0/F = 1 + K_{SV}[Q] = 1 + k_q \tau_0 [Q] \quad (4)$$

where the fluorescence intensity F decreases as a function of the quencher concentration [Q] and $F_0$ corresponds to the fluorescence intensity in absence of quencher. $K_{SV}$, $k_q$ and $\tau_0$ are the Stern-Volmer quenching constant, the quenching rate constant and the fluorescent lifetime of the biomolecule in absence of quencher, respectively [15].

In many cases the fluorescent biomolecule can be quenched, not only by collisions, but also by complex formation with the quencher, what is called static quenching. In those cases, an upward curvature in the plot of $F_0/F$ *vs*. [Q] is commonly observed [15]. Fluorescence lifetime measurements also allow analysing the contribution of the static mechanism. $\tau_0$ is only affected by the dynamic quenching, while the static mechanism does not produce changes in $\tau_0$ [15]. For static quenching, the relationship between fluorescence intensity and [Q] is described by the following equation

$$log \frac{(F_0 - F)}{F} = \log K_a + n \log[Q] \quad (5)$$

where *n* is the number of binding sites and $K_a$ corresponds to the binding constant [17-19].

### 2.4. Density functional theory (DFT) calculation details

DFT calculations were carried out to assign the BI-2536 spectra recorded at different pHs and analyze the neutral and protonated states of the drug. A previous thorough conformational analysis involving up to 14 different conformers was carried out for the neutral state of BI-2536 in gas phase to obtain the lowest energy conformation. The protocol consisted of two steps, i.e. (i) random conformational search with Avogadro [20] and (ii) geometry optimization of the lowest energy conformers, obtained in the previous step, with Gaussian (revision C.01) [21]. The nature of the stationary points was assessed by means of the normal vibration frequencies calculated from the analytical second derivatives of the energy. PBE0 method [22,23] as implemented in Gaussian09 along with the 6-31G* and 6-31+G** basis sets were used for the conformational analysis and the subsequent optimization of the molecular structure of BI-2536 in its neutral and protonated states. The 6-31+G** basis set is especially recommended in calculations involving anionic species [24]. Polarizable Continuum Model (PCM) was employed to include the solvent (water) effect [25,26].

$\Delta G^0$ was calculated for different protonation equilibria of BI-2536 to analyse their thermodynamics. A free energy of -270.28 kcal $mol^{-1}$ in aqueous solution was used for the solvation energy of the proton following the recommendation of Camaioni and Schwerdtfeger [27]. For the most thermodynamically-favoured species, the electronic transitions were calculated at the time-dependent (TD)-PBE0/6-31+G** level (including solvent effects). TD-PBE0 has previously been successfully employed to calculate low-

energy transitions for conjugated organic compounds when solvent effects are taken into account through the PCM approach [28-31].

### 2.5. Docking methodology

The program Autodock Vina [32] as implemented within Chimera [33] was initially applied to the experimental X-Ray structure of the complex HSA-warfarin in order to check the suitability of our docking protocol. Thus, the initial X-Ray structure, PDB code 2BXD [11], was downloaded into Chimera from the Protein Data Bank [34]. The system was prepared with the Dock Prep utility of Chimera with default parameters. This utility prepared both the protein and ligand adding missing hydrogens and assigning charges (Amber ff14SB charges for the protein and AM1-BCC charges for the ligand). Taking into account that the $pK_a$ of warfarin is 5.08 a total charge of -1 was assigned to warfarin. Once the ligand and receptor were prepared Autodock Vina was run defining a search box of 20 $Å^3$ around a central C of warfarin, with default parameters for ligand and receptor, requiring 10 binding modes with exhaustiveness of search equal to 8. Flexibility of sidechains of the receptor was not taken into account. The initial HSA/BI-2536 complex was manually constructed superimposing the pteridine core of BI-2536 to the chromene core of warfarin in the experimental HSA-warfarin complex, using as initial conformation for BI-2536 that determined by the DFT calculations. The preparation and docking processes used the same protocol as before, and a total charge of 0 was assigned to BI-2536.

A second step was conducted on the 10 obtained docked structures for the HSA/BI-2536 complex by means of the Amber 14 suite of programs [35]. Thus, each of the 10 complexes were prepared with the Antechamber and Leap modules of the AmberTools14 [35] package, using the Amber ff14SB [36] and gaff [37] force fields for

the protein and the ligand, respectively. Periodic boundary conditions through the particle-mesh Ewald method [38] for the treatment of the long-range electrostatic interactions were applied, and a cut-off distance of 9 Å was selected to compute non-bonded interactions. The solvent was considered explicitly using TIP3P [39] water molecules with a minimum distance from the edge of the box of 15 Å and removing those water molecules closer than 2.2 Å from any atom. Complexes were energy minimized with the sander module of Amber 14 [35] following a three steps protocol which first minimizes only water molecules, counterions and the ligand (5000 steepest descent steps), later also side chains are allowed to move (5000 steepest descent steps), and ends with 5000 (steepest descent) steps allowing the whole system to move.

Minimized structures were employed to predict the binding free energy ($\Delta G_{bind}$) of each of the predicted poses of warfarin and BI-2536 docked to HSA according to the MMPBSA and MMGBSA methodologies, as implemented in the MMPBSA.py module of the AmberTools 14 package [35]. Thus, the binding free energy is computed as the difference

$$\Delta G_{bind} = \Delta G_{complex} - (\Delta G_{protein} + \Delta G_{ligand}) \quad (6)$$

and each term can be estimated as follows

$$\Delta G = \Delta G^0 + \Delta G_{sol} = \Delta H^0_{MM} - T\Delta S^0 + \Delta G_{sol} \quad (7)$$

with the 0 superscript referring to values *in vacuo*, being $\Delta H^0_{MM}$ the molecular mechanics energy, $\Delta G_{sol}$ the solvation free energy, and $T\Delta S^0$ the entropic contribution. Taking into account the high computational cost to obtain the entropic term, it was not calculated and these results should be analysed as relative. The molecular mechanics energy is in turn calculated as a sum of the internal, electrostatic and van der Waals interactions:

$$\Delta H^0_{MM} = \Delta H^0_{int} + \Delta H^0_{ele} + \Delta H^0_{vdw} \quad (8)$$

while the solvation free energy is obtained from the polar and nonpolar contributions

$$\Delta G_{sol} = \Delta G_{ele,sol} + \Delta G_{nonpol,sol} \quad (9)$$

The polar contribution to solvation free energy can be calculated by solving the Poisson-Boltzmann (PB) equations [40] in the case of MMPBSA (using values of 1 and 80 for the interior and exterior dielectric constants, respectively), or by using the generalized Born (GB) approach (option igb=5 as implemented in Amber 14) [41] for MMGBSA.

Finally, the nonpolar contribution to solvation free energy is determined through the solvent accessible area (SASA, $Å^2$) according to

$$\Delta G_{nonpol,sol} = \gamma \, SASA + b \quad (10)$$

where $\gamma$ and $b$ are both assigned default values.

## 3. Results and discussion

### 3.1. Spectroscopic characterization and deprotonation equilibria of BI-2536

Fig. 2 shows the UV-Vis absorption spectra of BI-2536 recorded in different solvents. The absorption maximum ($\lambda_{ab}^{max}$) of BI-2536 corresponds to the HOMO→LUMO ($\pi,\pi^*$) transition and is slightly red-shifted in polar solvents (see Table 1). Nevertheless, a strong red-shift of the fluorescence emission maximum in polar solvents was observed (see Fig. 3 and Table 1). This may be due to stabilization of the excited state in polar solvents that in donor-acceptor molecules is generally associated to intramolecular charge transfer processes.

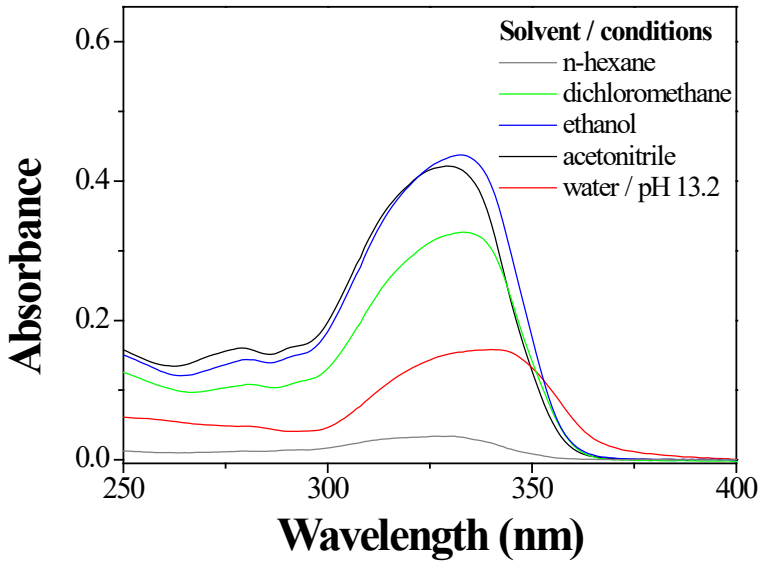


**Fig. 2.** UV-Vis absorption spectra of BI-2536 in different solvents (concentration of the samples was 10 μM).

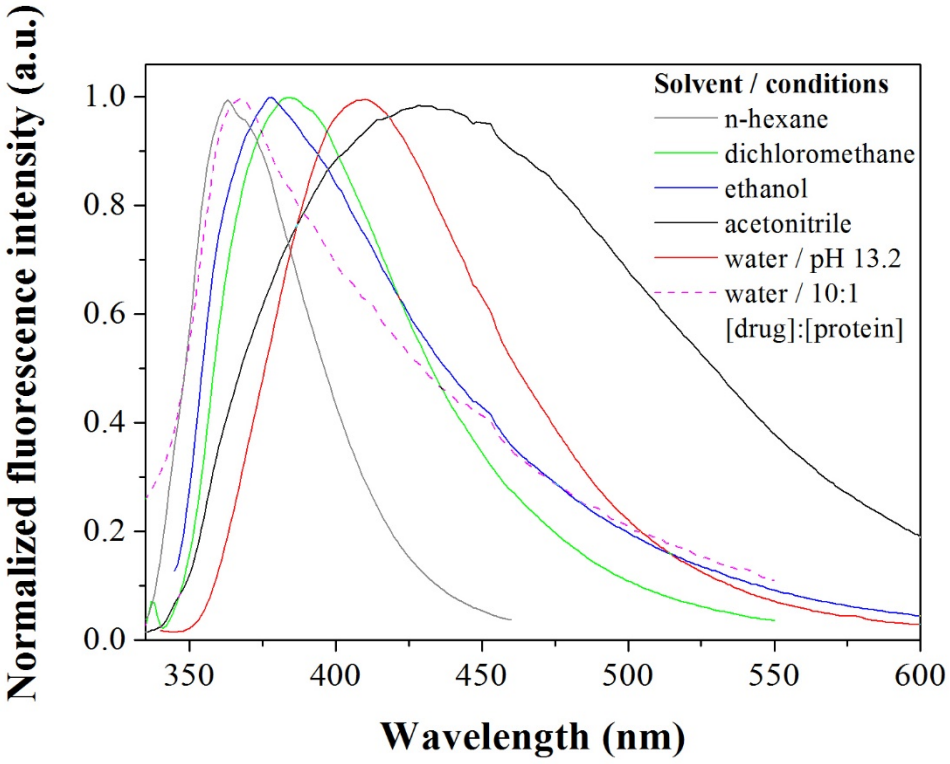


**Fig. 3.** Fluorescence emission spectra of BI-2536 in different solvents. Concentration of the samples was 10 μM with the exception of the mixture of BI-2536 (50 μM) and HSA (5 μM).

**Table 1**
Maximum absorption and emission wavelengths ($\lambda_{ab}^{max}$ and $\lambda_{em}^{max}$) found for BI-2536 in different solvents.

| Solvent | $\lambda_{ab}^{max}$ (nm) | $\lambda_{em}^{max}$ (nm) |
|---|---|---|
| n-hexane | 324 | 363 |
| dichloromethane | 333 | 382 |
| ethanol | 331 | 377 |
| acetonitrile | 328 | 428 |
| water (pH ≥ 13) | 340 | 410 |

In water solution, three different absorption spectra were recorded for BI-2536 at different pH values and fluorescence emission was only observed at pH ≥ 13 (see Fig. 3 and 4). In contrast, the fluorescence signal of BI-2536 was detected in presence of HSA at pH = 7.4 (see Fig. 3). This interesting behaviour along with the deprotonation equilibria of BI-2536 was investigated before carrying out binding experiments between BI-2536 and HSA. BI-2536 is a molecule containing some secondary and tertiary amino groups and, therefore, it can accept a variable number of protons as a function of the pH of the medium. Chart 1 shows the five protonation sites excluding the nitrogen atoms belonging to amide groups. In table 2, $\Delta G_i$, $\Delta G_{ij}$ and $\Delta G_{ijk}$ correspond to the Gibbs free energy difference of the first, second and third protonation equilibria, respectively, being i, j and k the protonation sites as numbered in Chart 1 (for the position 1 two different enantiomeric products, 1a and 1b, were also calculated). Product 3 (monoprotonated state), product 34 (diprotonated state) and product 345 (triprotonated state) are the most thermodynamically favoured species on the basis of the values obtained for $\Delta G$ of the different protonation equilibria (see Fig. 5). Table 3 shows the lowest electronic transitions calculated for the neutral and protonated forms of BI-2536. Very close energies were found for the electronic transitions of the neutral and monoprotonated forms and therefore the absorption spectrum of the species 1 which appears at pH ≥ 13 cannot be exclusively assigned to any of the two protonation states (see Fig. 4). The limited contribution of the terminal 1-methylpiperidine ring to the frontier molecular

orbitals (see Fig. 5) results in the similarity of the spectra of the neutral and monoprotonated forms. Species 2 appears within the range of pH 5-12 and was assigned to the diprotonated form of the drug (product 34). The protonation at position 4 results in a conjugation breaking, a blue-shift of the absorption band and the loss of the fluorescence signal. Finally, the absorption spectrum observed for the species 3 at pH ≤ 5 was assigned to the triprotonated form of the drug (product 345).

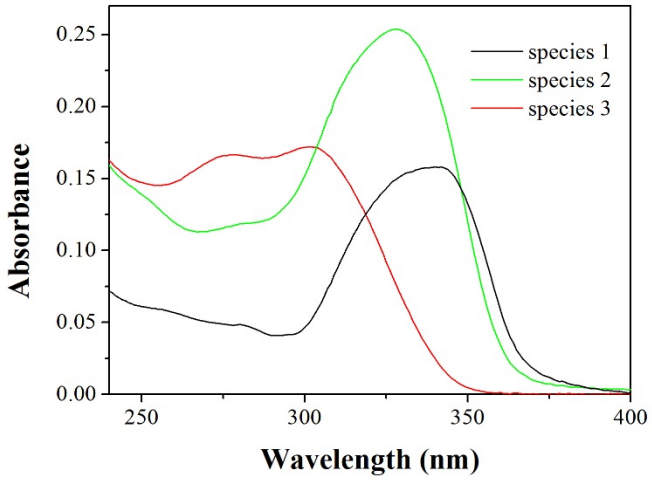


**Fig. 4.** UV-Vis absorption spectra of BI-2536 at different pHs (concentration of the samples was 10 μM). Species 1 at pH ≥ 13; species 2 within the range of pH 5-12; and species 3 at pH ≤ 5.

**Table 2**
Gibbs free energy calculated for the different protonation equilibria.

| Protonation equilibria | Product | $\Delta G_i$ (kcal mol$^{-1}$) | $\Delta G_{ij}$ (kcal mol$^{-1}$) | $\Delta G_{ijk}$ (kcal mol$^{-1}$) |
|---|---|---|---|---|
| First | 1a | 17.9 | | |
| | 1b | 25.2 | | |
| | 2 | 17.3 | | |
| | 3 | -6.9 | | |
| | 4 | -1.2 | | |
| | 5 | 7.6 | | |
| Second | 31a | | 19.0 | |
| | 31b | | 26.6 | |
| | 32 | | 20.0 | |
| | 34 | | -0.1 | |
| | 35 | | 8.2 | |
| Third | 341a | | | 36.9 |
| | 341b | | | 43.0 |
| | 342 | | | 37.9 |
| | 345 | | | 25.6 |

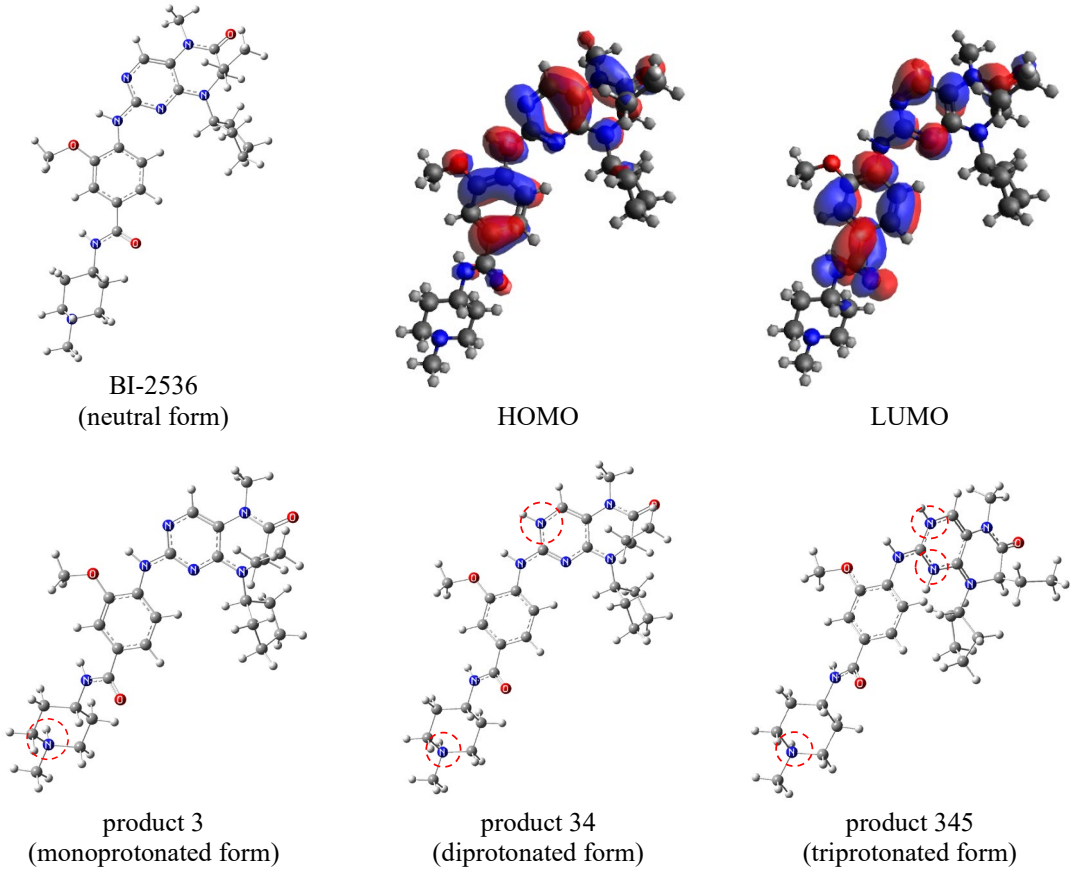


**Fig. 5.** Optimized molecular geometry of BI-2536 and its protonated forms. Frontier molecular orbitals of BI-2536 are also shown

**Table 3**
Electronic transitions computed for BI-2536 in neutral, monoprotonated, diprotonated and triprotonated forms at the TD-PBE0/6-31+G* level of theory including solvation effects.

| chemical species | E (eV [nm]) | E (eV [nm]) | *f* | main component of the transition (% contribution) |
|---|---|---|---|---|
| | *Experimental* | *Calculated* | | |
| neutral | 3.65 [340] | 3.73 [332] | 0.9132 | HOMO→LUMO (95%) |
| | | 4.11 [301] | 0.1985 | HOMO→LUMO+1 (88%) |
| monoprotonated | 3.65 [340] | 3.70 [335] | 0.9103 | HOMO→LUMO (95%) |
| | | 4.12 [301] | 0.1832 | HOMO→LUMO+1 (87%) |
| diprotonated | 3.78 [328] | 3.77 [328] | 0.1936 | HOMO→LUMO (97%) |
| | | 3.99 [310] | 0.8647 | HOMO→LUMO+1 (97%) |
| triprotonated | 4.13 [300] | 3.56 [348] | 0.0709 | HOMO→LUMO (98%) |
| | | 4.16 [298] | 0.3574 | HOMO→LUMO+1 (97%) |

303

304 **3.2. Fluorescence quenching of HSA by BI-2536 and binding site**

305 Fig. 6 shows a large decrease in the HSA fluorescence intensity as a function of the BI-
306 2536 concentration where the fluorescence signal of the protein practically disappears for
307 the [BI-2536]:[HSA] ratio of 10:1. This strong quenching suggests that the drug closely
308 interacts with the single tryptophan residue at the distal end of the site 1 pocket [9,11,42].
309 This assumption was also confirmed by competitive binding studies with warfarine and
310 ibuprofen (*vide infra*). Site 1 is a pre-formed binding pocket within the core of subdomain
311 IIA, is bigger than the binding site 2 and is predominantly apolar but contains two clusters
312 of basic and polar residues in the bottom and in the entrance of the pocket [9,11]. Different
313 non-charged drugs such as oxyphenbutazone and phenylbutazone bind to the site 1 pocket
314 and all of them have a planar group pinned snugly between the apolar side-chain of
315 Leu238 and Ala291 [11]. Some small drugs with acid groups such as 3-carboxy-4-
316 methyl-5-propyl-2-furanpropanoic acid (CMPF) also bind to site 1 in which some the
317 basic residues produce a charge neutralization and hydrogen bonding interactions with
318 acidic ligand [11]. Consequently, BI-2536 should not be able to bind directly to site 1
319 since it is a basic drug and is mainly protonated at the working pH. Nevertheless, a new
320 band centred at about 370 nm emerges with the increase of BI-2536 concentration in
321 presence of HSA (see Fig. 6) and corresponds to the fluorescence of BI-2536 which does
322 not emit light in its diprotonated form at pH = 7.4. Hence, the fluorescence of BI-2536 in
323 presence of HSA may be originated by the binding of non-protonated BI-2536 molecules
324 to hydrophobic pockets of the protein. In that case, a heterogeneous equilibrium in which
325 the non-protonated BI-2536 molecules are removed from the aqueous medium and bound
326 to the protein should be stablished. That should cause an equilibrium shift and the
327 deprotonation of new drug molecules. In the hydrophobic environment of the protein, the

non-protonated BI-2536 molecule emits fluorescence and, consequently, the maximum emission of BI-2536 in an apolar solvent such as *n*-hexane is close to that observed for a HSA (5 μM) and BI-2536 (50 μM) solution, in which the fluorescence of the protein has been almost quenched. The binding stoichiometry for the HSA/BI-2536 complex was analysed by the Jobs plot experiment (see Fig. 7) [43]. In that plot, the fluorescence intensity of different protein/drug mixtures was measured (solutions at different molar fraction of drug, $x_{BI2536}$, and total concentration [HSA] + [BI-2536] = 5 μM). The samples were excited at 340 nm and emission signal was collected at 420 nm. Consequently, the fluorescence intensity should mainly correspond to BI-2536 bound to HSA. The prominent increase of the fluorescence intensity is observed at the equimolar concentrations of protein and drug and, hence, HSA should have approximately one binding site for BI-2536.

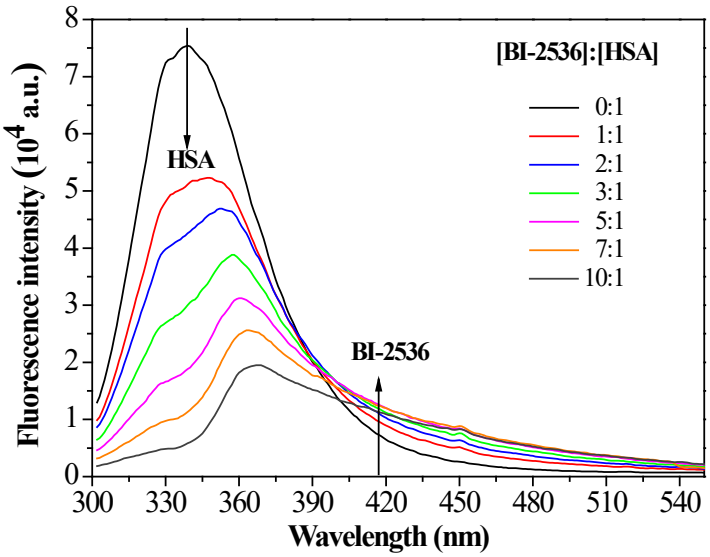


**Fig. 6.** Effect of BI-2536 on the fluorescence emission spectrum of HSA (T = 310 K, $\lambda_{exc}$ = 295 nm). [HSA] = 5 μM; [BI-2536] = 5-50 μM.

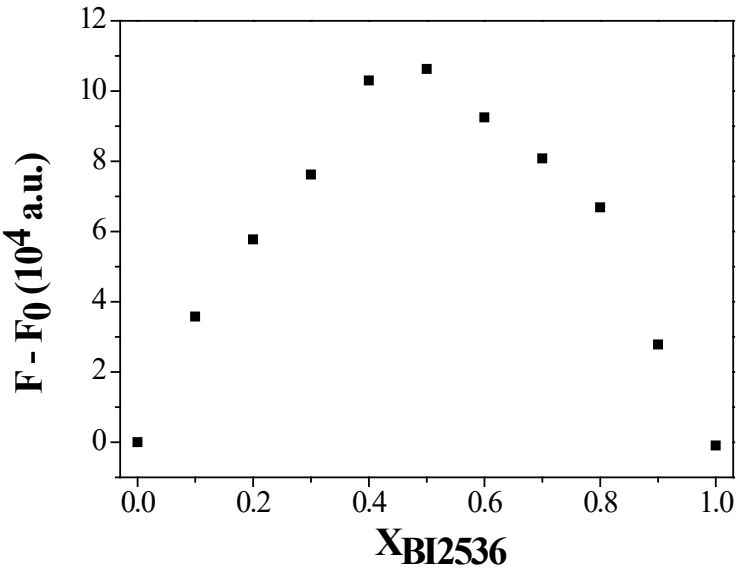


**Fig. 7.** Job plot for the complexation of BI-2536 and HSA. F corresponds to the fluorescence intensity of a solution of drug and protein at the molar fraction $x_{BI2536}$. $F_0 = F_{HSA,0} + F_{BI2536,0}$ corresponds to the sum of the fluorescence intensity of a free protein solution ($F_{HSA,0}$) and a free drug solution ($F_{BI2536,0}$) at the molar fraction $x_{BI2536}$. The total concentration was 5 μM ([HSA] + [BI-2536]) and the excitation and emission wavelengths were 340 and 420 nm, respectively.

Stern-Volmer plots of fluorescence quenching at different temperatures show upward curvature, which is generally attributed to the existence of static quenching (see Fig. 8) [15]. Curved Stern-Volmer plots have been observed for different fluorescence quenchers of serum albumins such as phenols, flavonoids, isoflavones and hydroxycinnamic acids [44-49]. Apart from the static quenching, charges in the fluorophore and quencher as well as the formation of closely spaced fluorophore-quencher pairs (which are not ground-state complexes but are immediately quenched and appear to be dark complexes) can also produce deviations from the classical Stern-Volmer equation [15]. The study of the dependence of the protein fluorescence lifetime with the quencher concentration, [Q], is also useful to estimate the relative contribution of the static mechanism, because fluorescence lifetime is usually only affected by the dynamic quenching [15]. Fig. 9 shows the fluorescence intensity decay for HSA in the presence of the drug in a [BI-2536]:[HSA] ratio of 5:1. Fluorescence decay data measured for HSA

in the absence and presence of the drug at 298 K are collected in Table 4. Fluorescence intensity decays were fitted to a tri-exponential function (n = 3 in eqn. (2)) and the distribution of the weighted residuals was random. A mean fluorescence lifetime, $\tau_m$, of 4.44 ns has been determined for free HSA at 298 K in our laboratory ($\lambda_{exc}$ = 291 nm; $\lambda_{em}$ = 320 nm). This value is lower than other previously reported fluorescence lifetimes for HSA (6.58 ns) measured at 293 K by Tayed et al. since the three-dimensional protein structure and, therefore, the fluorescence decay are in general dramatically affected by temperature [42]. No significant variations in the $\tau_m$ of the protein was observed in presence of BI-2536 (see Table 4). The low incidence of the collisional quenching to TRP214 seems to suggest that the diprotonated form of BI-2536, the major species in solution, cannot penetrate directly into the binding site.

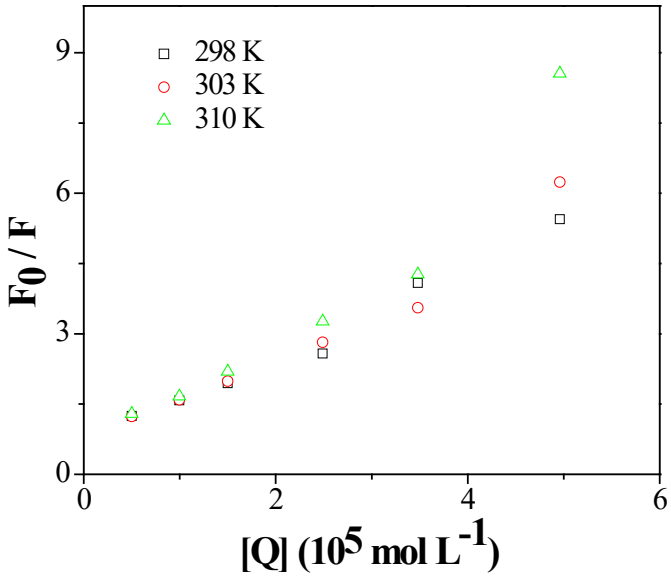


**Fig. 8**. Stern-Volmer plots for the binding of BI-2536 to HSA (5μM). Steady state fluorescence experiments at different temperatures.

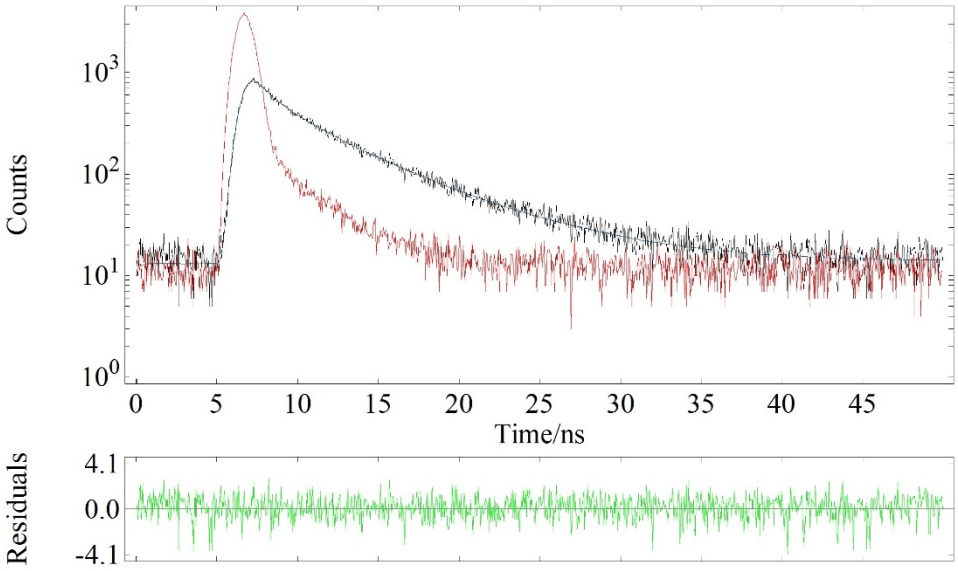


**Fig. 9.** Fluorescence intensity decay of HSA (1 μM) in the presence of the ligand in a [BI-2536]:[HSA] ratio of 5:1 at 298 K. The black line corresponds to the fluorescence decay of the sample and the red line is the instrument response function (IRF). The green line represents the distribution of the weighted residuals.

**Table 4**
Fluorescence decay data measured for HSA in the absence and presence of BI-2536 (298 K).

| [BI-2536]:[HSA] | $\tau_1$ (ns) | $\tau_2$ (ns) | $\tau_3$ (ns) | $\alpha_1$ x $10^{-3}$ | $\alpha_2$ x $10^{-3}$ | $\alpha_3$ x $10^{-3}$ | $\chi^2$ | $\tau_m$(ns) | $\tau_0 / \tau$ |
|---|---|---|---|---|---|---|---|---|---|
| 0:1 | 0.4698 | 2.358 | 6.094 | 12.47 | 5.918 | 5.177 | 1.129 | 4.437 | |
| 1:1 | 0.3822 | 2.060 | 6.130 | 9.215 | 4.836 | 3.721 | 1.168 | 4.455 | 0.996 |
| 2:1 | 0.4114 | 2.433 | 6.268 | 8.550 | 3.542 | 2.697 | 1.145 | 4.421 | 1.008 |
| 3:1 | 0.3302 | 2.100 | 6.317 | 6.338 | 3.368 | 2.193 | 1.155 | 4.477 | 0.987 |
| 5:1 | 0.5999 | 3.674 | 9.150 | 3.921 | 2.416 | 0.4866 | 1.071 | 4.768 | 0.939 |

## 3.3. Binding parameters of the HSA/BI-2536 complex

Binding parameters at different temperatures were determined according to eqn. (5) and an example is shown in Fig. 10. Corrected and uncorrected binding constants with eqn. (1), $K_a^c$ and $K_a^u$, along with the number of binding sites, *n*, are collected in Table 5 and 6. The values obtained for *n* indicate the existence of about one binding site on the HSA for BI-2536, being *n* dependent on the temperature. The increase of *n* with the temperature has been also observed for the binding of some other drugs such as dexamethasone and tenofovir [50-51]. The large differences observed between $K_a^c$ and $K_a^u$ show the

399 importance of correcting the fluorescence signal for inner effects of protein and drug.
400 Nevertheless, both binding constants will be used for comparative purposes. BI-2536
401 shows a strong affinity to HSA ($K_a^c = 3.78\times10^6$; $K_a^u = 1.14\times10^9$ at 310 K) in comparison
402 with the published binding constants of drugs which bind to site I such as warfarin ($K_a^u$
403 $= 6.17\times10^4$ at 310 K) [52], tenofovir ($K_a^u = 5.70\times10^4$ at 310 K) [51], dexamethasone ($K_a^u$
404 $= 7.1\times10^3$ at 308 K) and furosemide ($K_a^c = 1.99\times10^5$ at 310 K) [53]. Affinities to HSA
405 comparable to that of BI-2536 were found for two members of the imidazo[1,2-a]pyridine
406 family, with different known pharmaceutical applications ($K_a^c = 1.69\times10^6 – 4.28\times10^6$ at
407 310 K) [54]. Both those compounds and BI-2536 show a certain structural similarity, as
408 they are extended molecules with several aromatic rings. In general, the binding constants
409 to HSA reported for antioxidants such as flavonoids and phenolic acids ($K_a^u = 2.3\times10^4$
410 for quercetin and $K_a^u = 2.23\times10^4$ for ferulic acid; both at room temperature) are also lower
411 than that of BI-2536. In the competitive binding studies with ibuprofen (site 2 binder),
412 the binding constant did not vary significantly ($K_a^c = 2.29\times10^6$, at 310 K) (see Fig. 11).
413 Nevertheless, a strong decrease of the binding constant was observed for warfarin (site 1
414 binder) ($K_a^c = 2.78\times10^4$, at 310 K) supporting our previous assumption, that the
415 preferential binding site of BI-2536 corresponds to the site 1. The high binding constant
416 observed for the HSA/BI-2536 complex should bring on low concentration of free drug
417 in the blood plasma. Nevertheless, as previously mentioned, the complex would be
418 preferentially uptaken by tumours and might result in a higher drug concentration than in
419 other tissues.
420
421 **Table 5**
422 Binding parameters from the HSA/BI-2536 complex formation at different temperatures.
423

| T (K) | $n \pm 2\sigma$ | Log $K_a^c \pm 2\sigma$ |
|---|---|---|
| 310 | 1.35 ± 0.16 | 6.58 ± 0.88 |
| 303 | 1.30 ± 0.09 | 6.27 ± 0.36 |
| 298 | 1.22 ± 0.16 | 5.87 ± 0.74 |

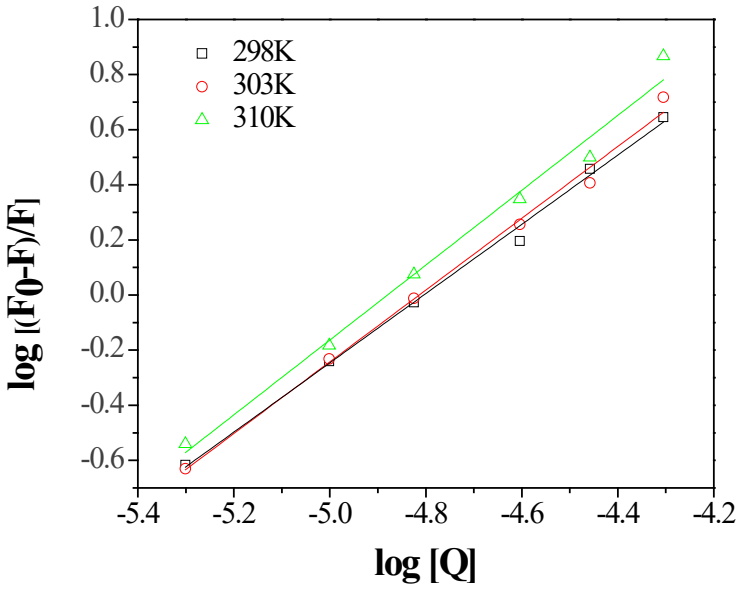


**Fig. 10.** Plot of log [($F_o$-F)/F] *vs*. log [Q] at different temperatures. Determination of $K_a^c$.

**Table 6**

Binding constants and thermodynamic parameters determined for the HSA/BI-2536 complex.

| T (K) | $K_a^c \times 10^{-6}$ | $K_a^u \times 10^{-8}$ | $\Delta H^0$ (KJ $mol^{-1}$) | $\Delta S^0$ (J $K^{-1}$ $mol^{-1}$) | $\Delta G^0$ (kJ $mol^{-1}$) |
|---|---|---|---|---|---|
| 310 | 3.78 | 11.4 | | | -39.2 |
| 303 | 1.86 | 2.08 | 103.8 | 461.3 | -36.0 |
| 298 | 0.745 | 0.554 | | | -33.6 |

(A)

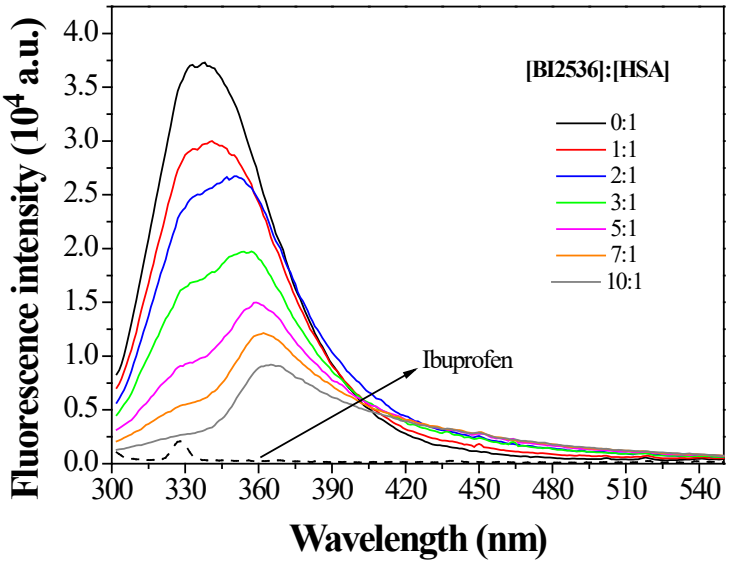


(B)

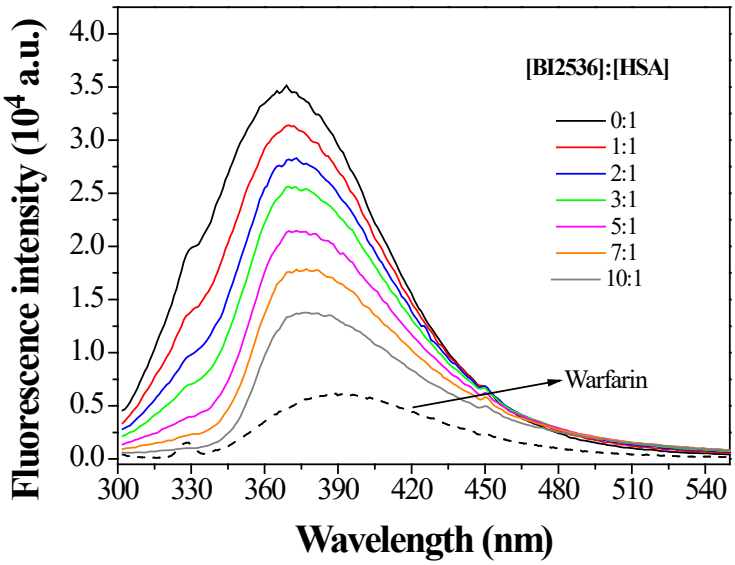


**Fig. 11.** Competitive binding studies with ibuprofen (A) and warfarin (b) (T = 310 K, $\lambda_{exc}$ = 295 nm, [HSA] = [competitive drug] = 5 μM; [BI-2536] = 5-50 μM.

### 3.4. Thermodynamic parameters and binding mode

Binding constants were determined at three different temperatures to study the thermodynamics of the formation of the HSA/BI-2536 complex. A strong dependence of

455 the affinity of BI-2536 to HSA with temperature was observed. $K_a^c$ exhibits a 5-fold
456 decrease when the temperature increases from 298 to 310 K. Enthalpy (ΔH) and entropy
457 (ΔS) changes for the binding process were obtained through the integrated van´t Hoff
458 equation:

459 $$Ln\ K_a = -\frac{\Delta H}{RT} + \frac{\Delta S}{R} \quad (11)$$

460 Fig. 12 shows the corresponding plot of Ln $K_a$ *vs.* $T^{-1}$ and Table 6 collects the
461 thermodynamic parameters obtained from the fitting (ΔH and ΔS). The free energy
462 change (ΔG) was calculated from the following equation:

463 $$\Delta G = \Delta H - T\Delta S \quad (12)$$

464 The binding process is exergonic although positive values were found for both ΔH and
465 ΔS. Hence, the binding process between BI-2536 and HSA is spontaneous and entropy-
466 driven. The positive values of ΔS could indicate that hydrophobic interactions are the
467 dominant ones in the complex formation [55,56]. The endothermic character of a drug –
468 protein association process is generally attributed to proton release or electrostatic
469 interactions [55,56]. As previously discussed, the interior of the site I pocket is
470 predominantly apolar [9,11] and, hence, the protonated forms of BI-2536 should not be
471 able to bind directly to site 1. In consequence the endothermic character of the association
472 process could be more related to proton release (from the protein or protonated drug) than
473 for electrostatic interactions.
474

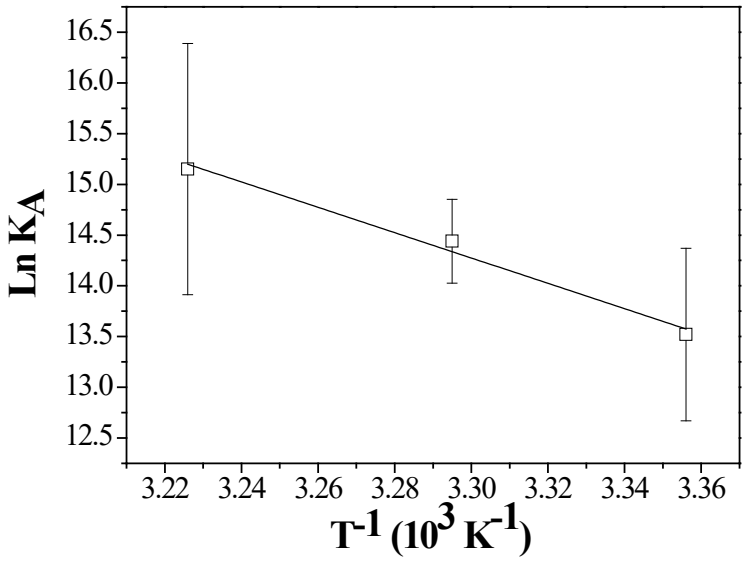


**Fig. 12.** Van´t Hoff plot for the binding of BI-2536 to HSA. Error bars correspond with ± σ.

The experimental results were used to perform a biased docking of BI-2536 to HSA in order to get a deeper insight into their possible interactions. Taking into account that BI-2536 seems to bind in the same pocket as warfarin, we first conducted a docking protocol on warfarin as a way of testing that our protocol is suitable. Fig. S1 (in Supplementary Data), which compares the docking poses of experimental and docked warfarin (best energy pose) allows to conclude that the protocol seems to be correct to be used with this system. Thus we used the experimental docking pose of warfarin as a starting model, as explained before, and considered the ligand to interact with the protein with a total charge of zero.

Table 7 summarizes the results after the docking, minimization and rescoring protocol with the MMPBSA and MMGBSA methodologies. Both MMPBSA and MMGBSA methodologies agree to predict poses 10, 3, 5 and 1 to be the best ones. Poses 1 and 10 are, indeed, very similar, as can be visualized in Fig. 13 and S2. Pose 3 is rotated 180º as compared with poses 1 and 10, while interacting with the same parts of HSA. On the contrary, pose 5 interacts with the protein in a completely different way.

**Table 7**

Calculated binding free energies (in kcal $mol^{-1}$) for each of the 10 proposed poses obtained with Autodock Vina and minimized with sander.

| Pose | $\Delta G_{bind}$(MMPBSA) | Pose | $\Delta G_{bind}$(MMGBSA) |
|---|---|---|---|
| 10 | -27.8 | 1 | -73.3 |
| 3 | -27.3 | 5 | -67.0 |
| 5 | -26.7 | 3 | -66.5 |
| 1 | -24.6 | 10 | -66.0 |
| 9 | -23.1 | 8 | -61.2 |
| 2 | -22.7 | 9 | -51.1 |
| 7 | -11.2 | 7 | -48.5 |
| 8 | -9.2 | 2 | -43.3 |
| 4 | -6.4 | 6 | -34.3 |
| 6 | -0.5 | 4 | -34.1 |

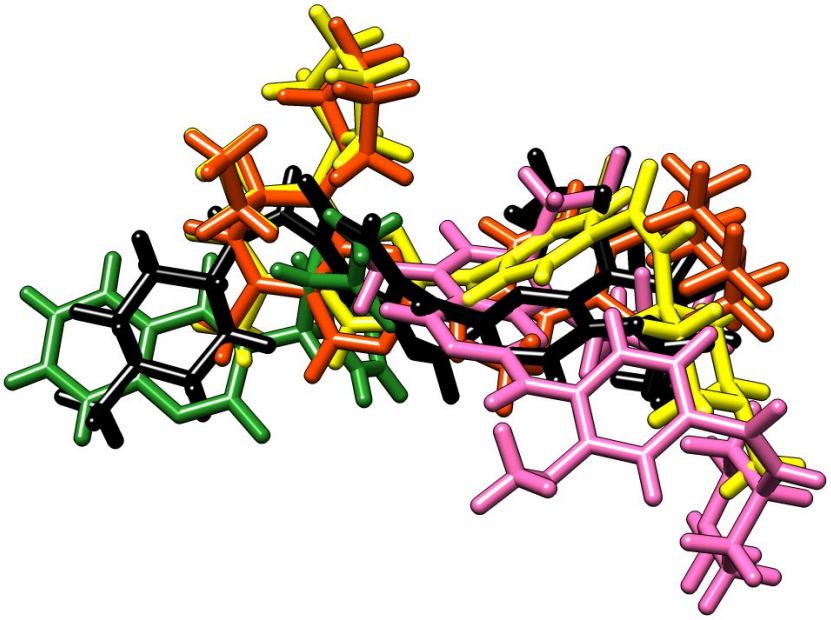

**Fig. 13.** Proposed docked structures for warfarin (green) and poses 1 (orange), 10 (yellow), 3 (black) and 5 (pink) of BI-2536.

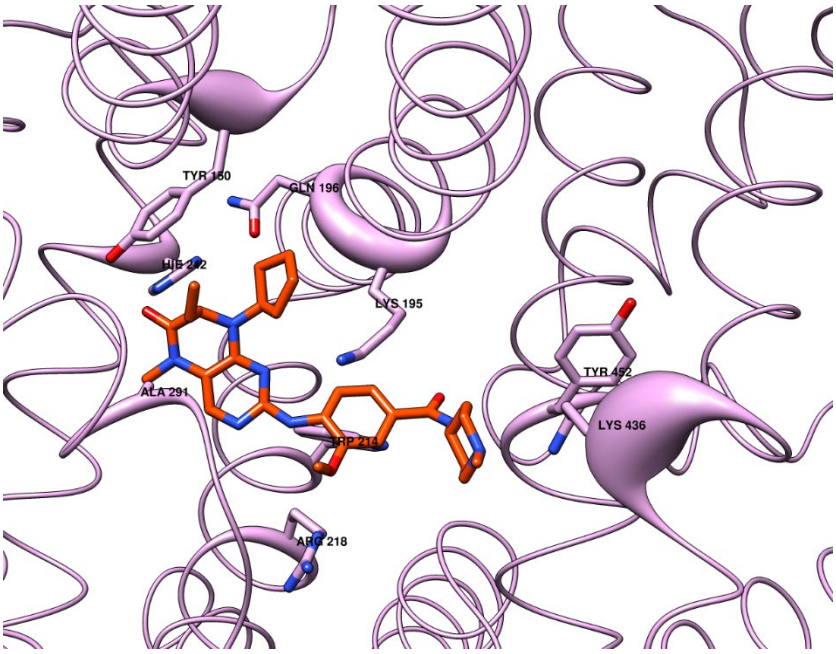


**Fig. 14.** Theoretical structure for pose 1 of BI-2536 docked to HSA, showing the protein with worm radii proportional to the MMGBSA predicted contribution of that residue to binding energy.

We thus further compared these 4 proposed BI-2536 poses by running a MMGBSA energy decomposition calculation, which allowed us to filter out which residues of HSA interact most with the ligand. Table 8 shows, defining a cut off of -1 kcal $mol^{-1}$, those residues for poses 1, 10, 3 and 5, along with the best pose of warfarin. TRP214 was included in all cases irrespective of its calculated interaction energy. These results can be visualized in an alternative way in Fig. 14 and Fig. S3-S6 (in ESI), which show the predicted structures using worm radii for HSA residues proportional to its contribution to binding energy. A global comparison for each of the proposed poses of the number of H-bonds established with the protein and the interaction energy of TRP214 (which according to the experimental results seems to interact with the ligand), together with a visual inspection and how these poses compare to the experimental structure of the HSA-warfarin complex, allows us to suggest pose 1 to be a feasible HSA/BI-2536 complex. This pose predicts that the main interactions between ligand and complex are of the van der Waals type ($\Delta G_{vdW}$ = -69.1 kcal $mol^{-1}$, $\Delta G_{ele}$= -41.8 kcal $mol^{-1}$ for pose 1 of BI-2536).

Our experimental results conclude that BI-2536 binds stronger to HSA than warfarin [52]. The proposed BI-2536 docked structure can be considered in fact an elongation of warfarin which is able of establishing new favourable interactions with the protein. These similarities and dissimilarities in their interaction with HSA can be easily visualized using Ligplot+ [57] (see Fig. 15). Fig. 15 allows to conclude also that the main interactions established between BI-2536 and HSA are of the van der Waals type. It seems also important for the ligands to have at least one oxygen as a substituent in the fused ring motif in order to establish an H-bond with His242. Besides, the bigger size of BI-2536 as compared to warfarin allows the first to establish a new H-bond with Arg218 and with Lys436.

**Table 8**
MMGBSA energy decomposition (in kcal $mol^{-1}$), showing those residues of HSA that interact most with the ligand. The H-bond column determines which of those residues are establishing an H-bond with the ligand.

| Compound | Pose | Residue | $\Delta G_{bind}$ | H-bond |
|---|---|---|---|---|
| BI-2536 | 1 | LYS436 | -5.4 | |
| | | TYR150 | -4.0 | YES |
| | | LYS195 | -2.9 | |
| | | HIS242 | -2.3 | YES |
| | | GLN196 | -2.2 | |
| | | ARG218 | -1.6 | YES |
| | | TYR452 | -1.6 | |
| | | ALA291 | -1.5 | |
| | | TRP214 | -1.2 | |
| BI-2536 | Pose 10 | TYR150 | -4.6 | YES |
| | | LYS195 | -2.5 | |
| | | CYS448 | -2.4 | |
| | | HIS242 | -2.1 | YES |
| | | LYS199 | -1.4 | YES |
| | | ALA291 | -1.2 | |
| | | TRP214 | -1.1 | |
| | | LEU238 | -1.0 | |
| BI-2536 | Pose 3 | ARG222 | -3.5 | |
| | | LYS199 | -3.2 | YES |
| | | GLU292 | -2.6 | |
| | | LYS195 | -1.6 | |
| | | TYR150 | -1.6 | |
| | | ALA291 | -1.5 | |
| | | LEU238 | -1.5 | |
| | | TRP214 | -1.4 | |
| BI-2536 | Pose 5 | ARG218 | -7.4 | |
| | | CYS448 | -3.1 | |
| | | LYS444 | -2.0 | |

| | | | |
|---|---|---|---|
| | ARG222 | -2.0 | YES |
| | HIS440 | -1.9 | |
| | LYS195 | -1.6 | |
| | VAL343 | -1.2 | |
| | TRP214 | -0.9 | |
| | GLU292 | | YES |
| Warfarin | TYR150 | -5.0 | |
| | HIS242 | -3.9 | YES |
| | LEU238 | -2.5 | |
| | ARG222 | -2.5 | |
| | ALA291 | -2.2 | |
| | ILE290 | -1.5 | |
| | LEU260 | -1.4 | |
| | ARG257 | -1.1 | |
| | TRP214 | -0.5 | |

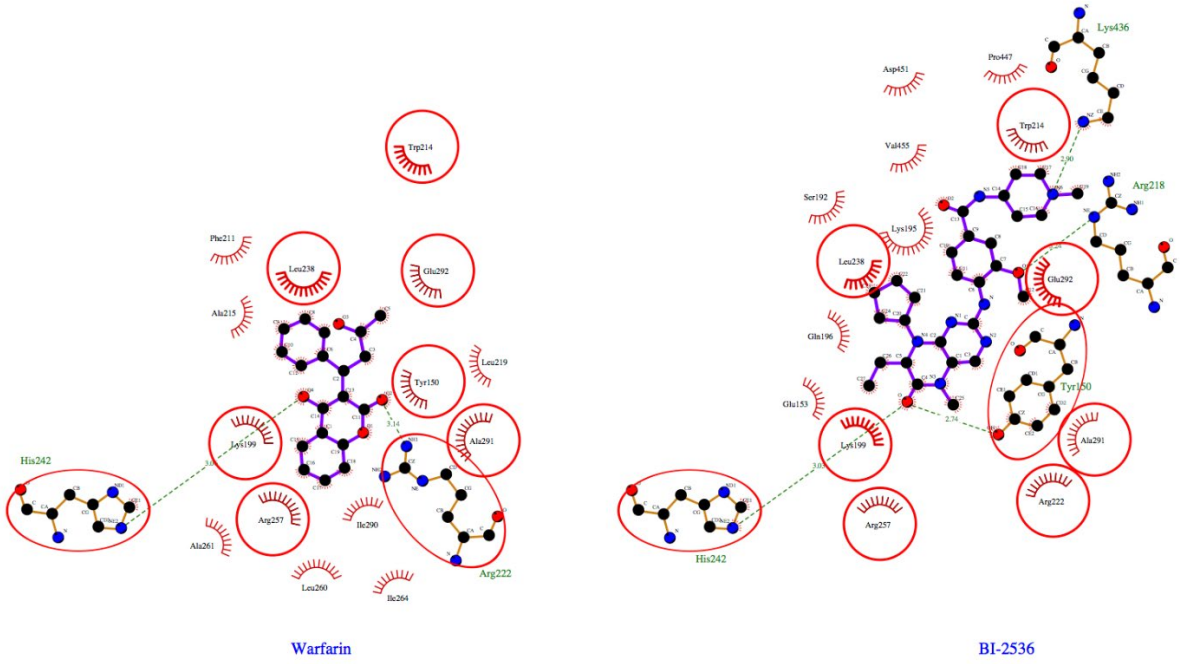


**Fig. 15.** Interactions established between the ligands warfarin and BI-2536 and the protein HSA. Shared interactions are circled in red.

## 3.5. Changes of the secondary structure of HSA induced by BI-2536

Fig. 16 shows the FTIR spectra recorded at room temperature for the free protein and for the HSA/BI-2536 complex in Tris-HCl buffer solution. For free HSA, the protein amide I and amide II bands appear at 1652 $cm^{-1}$ and 1547 $cm^{-1}$, respectively. These bands are mainly attributed to C=O stretching and N–H in plane deformation coupled with C–N stretching, respectively [58-61]. Both peaks, but particularly the first one, are related to

555 the secondary structure of proteins. Amide I consists of many overlapping component
556 bands that represent different structural elements, i.e. α-helices, β-sheets, β-turns and
557 random coils. The bands within the range 1610 – 1640 $cm^{-1}$ are generally assigned to β-
558 sheet, 1640 – 1650 $cm^{-1}$ to random coil, 1650 – 1658 $cm^{-1}$ to α-helix and 1660 – 1700
559 $cm^{-1}$ to β-turn structure [58-60]. In general, no substantial changes were observed in the
560 FTIR spectrum of the protein in presence of the drug (in a ratio [BI-2536]:[HSA] of 1:1).
561 Fig. 14 shows the curve fit in the amide I region for the free protein and for the protein-
562 drug complex. The binding of BI-2536 to HSA does not result in a significant change of
563 the amount of α-helix (from 40.5 for the free HSA to 41.3% in presence of BI-2536). The
564 amounts of β-sheet and β-turn decreased from 40.1 to 36.8% and from 19.4 to 21.9%.
565 From these results, it can be inferred that the binding of BI-2536 to HSA does not result
566 in a large change of the secondary structure of the protein.
567
568
569
570
571
572
573
574
575
576
577
578
579

(A)

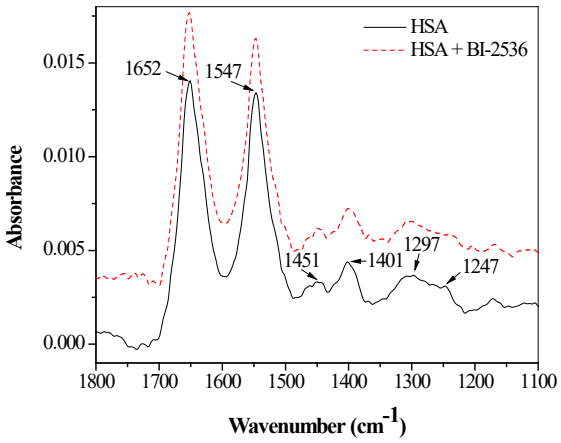


(B)

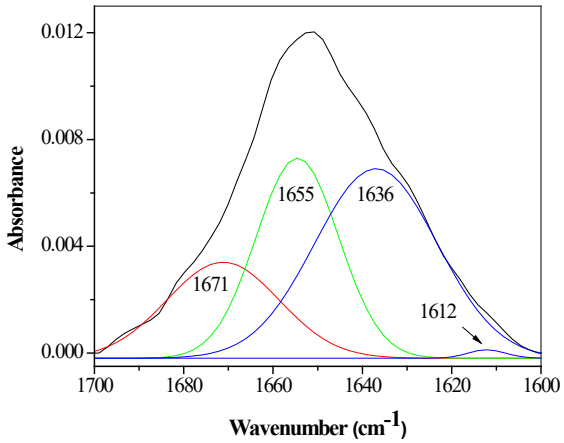


(C)

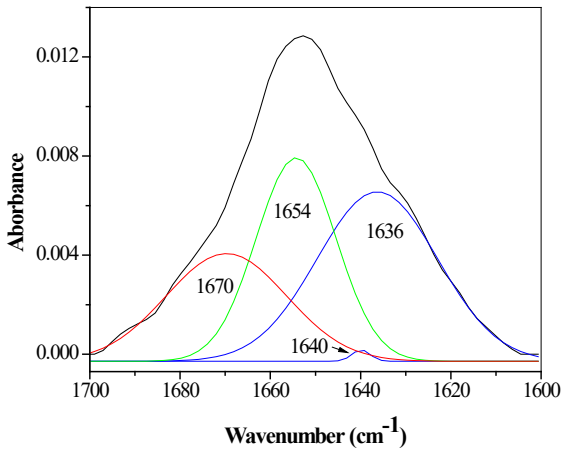


**Fig. 16.** (A) FTIR spectra of free HSA (solid line) and HSA/BI-2536 complex (dashed line) [(HSA+BI-2536) solution spectrum – BI-2536 solution spectrum] at room temperature (B) HSA/BI-2536 complex (C) HSA and BI-2536 concentrations used were of 1mM.

## 4. Conclusions

In this paper, the binding of the anticancer drug BI-2536 to HSA has been studied by means of different spectroscopic techniques and docking calculations. First of all, it was established that the diprotonated state (non-fluorescent) is the main form of the drug at the physiological pH of 7.4 by using UV-Vis absorption spectroscopy and DFT calculations. A set of quenching fluorescence experiments using the native fluoresce of HSA allows determining the binding constant of the complex HSA/BI-2536 at three different temperatures. In general, the binding constants determined for that complex are high in comparison to values reported for common drugs that bind to HSA such as warfarin, tenofovir, dexamethasone and furosemide. However, FTIR experiments showed that the binding did not result in a large change of the secondary structure of the protein. The strong quenching observed for the HSA/BI-2536 complex and the competitive binding studies with warfarin and ibuprofen indicate that the drug closely interacts with TRP214 at the distal end of the site 1 pocket. This is a hydrophobic pocket that should not allow the binding of BI-2536 in a charged state. On this assumption, only non-protonated BI-2536 molecules could bind within the pocket causing an equilibrium shift and the deprotonation of new molecules in the aqueous medium. As a result, BI-2536 emits fluorescence in presence of the protein despite the drug should be protonated (non-fluorescent) in the aqueous medium at the working pH. In addition, the Jobs plot experiment indicated that HSA should have only one binding site for BI-2536.

On the basis of the determined thermodynamic parameters for the binding process ($\Delta H > 0$, $\Delta S > 0$ and $\Delta G < 0$), it can be concluded that this process is spontaneous and entropy-driven. The endothermic character of the binding could be related to proton release processes. Calculations also showed that the main protein - drug interactions are

of the van der Waals type although the presence of amide and ether groups in BI-2536 allow H-bonding with some residues such as His242, Arg218 and Tyr150.

**Acknowledgements**

The authors would like to thank the Consejería de Educación y Ciencia de la Junta de Comunidades de Castilla-La Mancha (Project PEII11-0279-8538) for supporting the research described in this article and the University of Castilla-La Mancha for additional support of the research group (grants GI20152958 and GI20163548).

**References**

[1] P. Lénárt, M. Petronczki, M. Steegmaier, B. Di Fiore, J.J. Lipp, M. Hoffmann, W.J. Rettig, N. Kraut, J.M. Peters, The small-molecule inhibitor BI-2536 reveals novel insights into mitotic roles of polo-like kinase 1, Curr. Biology 17 (2007) 304–315.

[2] M. Steegmaier, M. Hoffmann, A. Baum, P. Lénárt, M. Petronczki, M. Krššák, U. Gürtler, P. Garin–Chesa, S. Lieb, J. Quant, M. Grauert, G.R. Adolf, N. Kraut, J.M. Peters, W.J. Rettig, BI-2536, a potent and selective inhibitor of polo-like kinase 1, inhibits tumor growth in vivo, Curr. Biology 17 (2007) 316–322.

[3] H. Yim, Current clinical trials with polo-like kinase 1 inhibitors in solid tumors, Anticancer Drugs 10 (2013) 999–1006.

[4] L. Garuti, M. Roberti, G. Bottegoni, Polo-like kinases inhibitors, Curr. Med. Chem. 19 (2012) 3937–3948.

[5] K.S. Lee, T.R. Burke Jr, J. Park, J.K. Bang, E. Lee, Recent Advances and New Strategies in Targeting Plk1 for Anticancer Therapy, Trends. Pharmacol. Sci. 36 (2015) 858-877.

637 [6] P. Lahiry, A. Torkamani, N.J. Schork, R.A. Hegele, Kinase mutations in human
638 disease: interpreting genotype-phenotype relationships, Nat. Rev. Genet. 11 (2010)
639 60–74.
640 [7] G. Fanali, A. di Masi, V. Trezza, M. Marino, M. Fasano, P. Ascenzi, Human serum
641 albumin: From bench to bedside, Mol. Asp. Med. 33 (2012) 209–290.
642 [8] M. Fasano, S. Curry, E. Terreno, M. Galliano, G. Fanali, P. Narciso, S. Notari, P.
643 Ascenzi, The extraordinary ligand binding properties of human serum albumin,
644 IUBMB Life 57 (2005) 787–796.
645 [9] F. Yang, Y. Zhang, H. Liang, Interactive Association of Drugs Binding to Human
646 Serum Albumin, Int. J. Mol. Sci. 15 (2014) 3580–3595.
647 [10] K. Yamasaki, V.T. Chuang, T. Maruyama, M. Otagiri, Albumin–drug interaction
648 and its clinical implication, Biochim. Biophys. Acta 1830 (2013) 5435–5443.
649 [11] J. Ghuman, P.A. Zunszain, I. Petitpas, A.A. Bhattacharya, M. Otagiri, S. Curry,
650 Structural Basis of the Drug-binding Specificity of Human Serum Albumin, J. Mol.
651 Biol. 353 (2005) 38–52.
652 [12] F. Kratz, Albumin as a drug carrier: Design of prodrugs, drug conjugates and
653 nanoparticles, J. Controlled Release 132 (2008) 171–183.
654 [13] G. Lambrinidis, T. Vallianatou, A. Tsantili–Kakoulidou, In vitro, in silico and
655 integrated strategies for the estimation of plasma protein binding, Advanced Drug
656 Delivery Reviews 86 (2015) 27–45.
657 [14] A.M. Merlot, D.S. Kalinowski, D.R. Richardson, Unraveling the mysteries of
658 serum albumin—more than just a serum protein, Front. Physiol. 5 (2014) 299.
659 [15] J.R. Lakowicz, Principles of Fluorescence Spectroscopy, third ed., Springer, New
660 York, 2006.

[16] S. Sugio, A. Kashima, S. Mochizuki, M. Noda, K. Kobayashi, Crystal structure of human serum albumin at 2.5 Å resolution, Protein Eng. 12 (1999) 439–446.

[17] J. Ming, X. Meng–Xia, Z. Dong, L. Yuan, L. Xiao–Yu, C. Xing, Spectroscopic studies on the interaction of cinnamic acid and its hydroxyl derivatives with human serum albumin, J. Molec. Struct. 692 (2004) 71–80.

[18] M. Zhang, Q. Lv, N. Yue, H. Wang, Study of fluorescence quenching mechanism between quercetin and tyrosine-$H_2O_2$-enzyme catalyzed product, Spectrochim. Acta Part A 72 (2009) 572–576.

[19] X.–Z. Feng, Z. Lin, L.–J. Yang, C. Wang, C.–L. Bai, Investigation of the interaction between acridine orange and bovine serum albumin, Talanta 47 (1998) 1223–1229.

[20] M.D. Hanwell, D.E. Curtis, D.C. Lonie, T. Vandermeersch, E. Zurek, G.R. Hutchison, Avogadro: An advanced semantic chemical editor, visualization, and analysis platform, Journal of Cheminformatics 4 (2012) 17.

[21] M.J. Frisch, G.W. Trucks, H.B. Schlegel, G.E. Scuseria, M.A. Robb, J.R. Cheeseman, J.A. Montgomery, J.T. Vreven, K.N. Kudin, J.C. Burant, J.M. Millam, S.S. Iyengar, J. Tomasi, V. Barone, B. Mennucci, M. Cossi, G. Scalmani, N. Rega, G.A. Petersson, H. Nakatsuji, M. Hada, M. Ehara, K. Toyota, R. Fukuda, J. Hasegawa, M. Ishida, T. Nakajima, Y. Honda, O. Kitao, H. Nakai, M. Klene, X. Li, J.E. Knox, H.P. Hratchian, J.B. Cross, C. Adamo, J. Jaramillo, R. Gomperts, R.E. Stratmann, O. Yazyev, A.J. Austin, R. Cammi, C. Pomelli, J.W. Ochterski, P.Y. Ayala, K. Morokuma, G.A. Voth, P. Salvador, J.J. Dannenberg, V.G. Zakrzewski, S. Dapprich, A.D. Daniels, M.C. Strain, O. Farkas, D.K. Malick, A.D. Rabuck, K. Raghavachari, J.B. Foresman, J.V. Ortiz, Q. Cui, A.G. Baboul, S. Clifford, J. Cioslowski, B.B. Stefanov, G. Liu, A. Liashenko, P. Piskorz, I. Komaromi, R.L.

686 Martin, D.J. Fox, T. Keith, M.A. AlLaham, C.Y. Peng, A. Nanayakkara, M.
687 Challacombe, P.M.W. Gill, B. Johnson, W. Chen, M.W. Wong, C. Gonzalez, J.A.
688 Pople, Gaussian 09, Revision C.01, Gaussian, Inc., Wallingford, CT, 2009.
689 [22] J.P. Perdew, K. Burke, M. Ernzerhof, Generalized Gradient Approximation Made
690 Simple, Phys. Rev. Lett. 77 (1996) 3865.
691 [23] C. Adamo, V. Barone, A TDDFT study of the electronic spectrum of s-tetrazine
692 in the gas-phase and in aqueous solution, Chem. Phys. Lett. 330 (2000) 152–160.
693 [24] J.B. Foresman, A.E. Frisch, Exploring chemistry with electronic structure
694 methods, second ed., Pittsburg: Gaussian. Inc, Pittsburgh,1996.
695 [25] M. Cossi, N. Rega, G. Scalmani, V. Barone, Energies, structures, and electronic
696 properties of molecules in solution with the C-PCM solvation model, J. Comput.
697 Chem. 24 (2003) 669–681.
698 [26] J. Tomasi, B. Mennucci, R. Cammi, Quantum Mechanical Continuum Solvation
699 Models, Chem. Rev. 105 (2005) 2999–3094.
700 [27] D. M. Camaioni, A. Schwerdtfeger, Comment on accurate experimental values
701 for the free energies of hydration of $H^+$, $OH^-$, and $H_3O^+$, J. Phys. Chem. A. 109 (2005)
702 10795–10797.
703 [28] D. Jacquemin, E.A. Perpète, G.E. Scuseria, I. Ciofini, C. Adamo, TD-DFT
704 Performance for the Visible Absorption Spectra of Organic Dyes: Conventional
705 versus Long-Range Hybrids, J. Chem. Theory Comput.4 (2008) 123–135.
706 [29] Garzón, J.M. Granadino–Roldán, M. Moral, G. García, M.P. Fernández–Liencres,
707 A. Navarro, T. Peña–Ruiz , M. Fernández–Gómez, Density functional theory study
708 of the optical and electronic properties of oligomers based on phenyl-ethynyl units
709 linked to triazole, thiadiazole, and oxadiazole rings to be used in molecular
710 electronics, J. Chem. Phys. 132 (2010) 064901.

711 [30] M. Moral, G. García, A. Peñas, A. Garzón, J.M. Granadino–Roldán, M. Melguizo,
712 M. Fernández–Gómez, Electronic properties of diphenyl-*s*-tetrazine and some related
713 oligomers. A spectroscopic and theoretical study, Chem. Phys. 408 (2012) 17–27.
714 [31] A. Garzón, I. Bravo, M.R. Carrión–Jiménez, A. Rubio–Moraga, J. Albaladejo,
715 Spectroscopic study on binding of gentisic acid to bovine serum albumin,
716 Spectrochim. Acta A Mol. Biomol.Spectrosc. 150 (2015) 26–33.
717 [32] O. Trott, A. J. Olson, AutoDock Vina: Improving the speed and accuracy of
718 docking with a new scoring function, efficient optimization, and multithreading, J.
719 Comput. Chem. 31 (2010) 455–461.
720 [33] E. F. Pettersen, T. D. Goddard, C. C. Huang, G. S. Couch, D. M. Greenblatt, E.
721 C. Meng, T. E. Ferrin, UCSF Chimera–A visualization system for exploratory
722 research and analysis, J. Comput. Chem. 25 (2004) 1605–1612.
723 [34] H. M. Berman, J. Westbrook, Z. Feng, G. Gilliland, T. N. Bhat, H. Weissig, I. N.
724 Shindyalov, P. E. Bourne, The Protein Data Bank, Nucleic Acids. Res. 28 (2000) 235–
725 242.
726 [35] D.A. Case, V. Babin, J.T. Berryman, R.M. Betz, Q. Cai, D.S. Cerutti, T.E.
727 Cheatham, T.A. Darden, R.E. Duke, H. Gohlke, A.W. Goetz, S. Gusarov, N.
728 Homeyer, P. Janowski, J. Kaus, I. Kolossváry, A. Kovalenko, T.S. Lee, S. LeGrand,
729 T. Luchko, R. Luo, B. Madej, K.M. Merz, F. Paesani, D.R. Roe, A. Roitberg, C.
730 Sagui, R. Salomon–Ferrer, G. Seabra, C.L. Simmerling, W. Smith, J. Swails, R.C.
731 Walker, J. Wang, R. M. Wolf, X. Wu, P.A. Kollman, AMBER 14, University of
732 California, San Francisco, 2014.
733 [36] V. Hornak, R. Abel, A. Okur, B. Strockbine, A. Roitberg, C. Simmerling,
734 Comparison of multiple Amber force fields and development of improved protein
735 backbone parameters, Proteins 65 (2006) 712–725.

[37] J. Wang, R.M. Wolf, J.W. Caldwell, P.A. Kollman, D.A. Case, Development and testing of a general amber force field, J. Comput. Chem. 25 (2004) 1157–1174.

[38] T. Darden, D. York, L. Pedersen, Particle mesh Ewald: An N·log(N) method for Ewald sums in large systems, J. Chem. Phys. 98 (1993) 10089–10092.

[39] W.L. Jorgensen, J. Chandrasekhar, J.D. Madura, R.W. Impey, M.L. Klein, Comparison of simple potential functions for simulating liquid water, J. Chem. Phys. 79 (1983) 926–935.

[40] W. Rocchia, E. Alexov, B. Honig, Extending the Applicability of the Nonlinear Poisson−Boltzmann Equation: Multiple Dielectric Constants and Multivalent Ions, J. Phys. Chem. B. 105 (2001) 6507–6514.

[41] A. Onufriev, D. Bashford, D.A. Case, Exploring protein native states and large-scale conformational changes with a modified generalized born model, Proteins 55 (2004) 383–394.

[42] N. Tayeh, T. Rungassamy, J.R. Albani, Fluorescence spectral resolution of tryptophan residues in bovine and human serum albumins, J. Pharm. Biomed. Anal. 50 (2009) 107–116.

[43] C.Y. Huang, Determination of binding stoichiometry by the continuous variation method: the Job plot, Methods Enzymol 87 (1982) 509–525.

[44] M. Wen, J. Tian, Y. Huang, H. Bian, Z. Chen, H. Liang, Interaction between Xanthoxylin and Bovine Serum Albumin, J. Chem. 27 (2009) 306–310.

[45] A. Papadopoulou, R.J. Green, R.A. Frazier, Interaction of Flavonoids with Bovine Serum Albumin: A Fluorescence Quenching Study, J. Agric. Food Chem. 53 (2005) 158–163.

[46] J. Zhao, F. Ren, Influence of hydroxylation and glycosylation in ring A of soybean isoflavones on interaction with BSA, Spectrochimica Acta Part A 72 (2009) 682–685.

761 [47] L. Trnková, I. Boušová, V. Kubíček, J. Dršata, Binding of naturally occurring
762 hydroxycinnamic acids to bovine serum albumin, Natur. Sci. 2 (2010) 563–570.
763 [48] J. Min, X. Meng-Xia, Z. Dong, L. Yuan, L. Xiao-Yu, C. Xing, Spectroscopic
764 studies on the interaction of cinnamic acid and its hydroxyl derivatives with human
765 serum albumin, J. Mol. Struct. 692 (2004) 71–80.
766 [49] H. Cao, D. Wu, H. Wang, M. Xu, Effect of the glycosylation of flavonoids on
767 interaction with protein, Spectrochim. Acta A. 73 (2009) 972–975.
768 [50] P.N. Naik, S.A. Chimatadar, S.T. Nandibewoor, Interaction between a potent
769 corticosteroid drug – Dexamethasone with bovine serum albumin and human serum
770 albumin: A fluorescence quenching and fourier transformation infrared spectroscopy
771 study, J. Photochem. Photobiol. B. 100 (2010) 147–159.
772 [51] N. Shahabadi, S. Hadidi, F. Feizi, Study on the interaction of antiviral drug
773 'Tenofovir' with human serum albumin by spectral and molecular modeling methods,
774 Spectrochim. Acta A. 138 (2015) 169–175.
775 [52] Q. Li, W.Y. Yang, L.L. Qu, H.Y. Qi, Y. Huang, Z. Zhang, Interaction of Warfarin
776 with Human Serum Albumin and Effect of Ferulic Acid on the Binding, J. Spectros.
777 (2014) 834501.
778 [53] N. Zaidi, E. Ahmad, M. Rehan, G. Rabbani, M.R. Ajmal, Y. Zaidi, N. Subbarao,
779 R.H. Khan, Biophysical insight into furosemide binding to human serum albumin: a
780 study to unveil its impaired albumin binding in uremia, J. Phys. Chem. B. 117 (2013)
781 2595–2604.
782 [54] A. Özdemir, E. Gökoğlu, E. Yılmaz, E. Yalçın, E. Gökoğlu, Z. Seferoğlu, T.
783 Tekinay, Investigation of binding properties of dicationic styrylimidazo[1,2-
784 a]pyridinium dyes to human serum albumin by spectroscopic techniques, Lumin. 32
785 (2017) 86-92.

[55] M. Klotz, Physiochemical aspects of drug-protein interactions: a general perspective, Ann. N. Y. Acad. Sci. 226 (1973) 18–35.

[56] P.D. Ross, S. Subramanian, Thermodynamics of Protein Association Reactions: Forces Contributing to Stability, Biochemistry 20 (1981) 3096–3102.

[57] R. A. Laskowski, M. B. Swindells, LigPlot+: multiple ligand-protein interaction diagrams for drug discovery, J. Chem. Inf. Model. 51 (2011) 2778–2786.

[58] S. Wi, P. Pancoska, T.A. Keiderling, Predictions of protein secondary structures using factor analysis on Fourier transform infrared spectra: effect of Fourier self-deconvolution of the amide I and amide II bands, Biospectroscopy 4 (1998) 93–106.

[59] J. Kong, S. Yu, Fourier Transform Infrared Spectroscopic Analysis of Protein Secondary Structures, Acta Biochim. Biophys. Sinica 39 (2007) 549–559.

[60] P. Garidel, H. Schott, Fourier-Transform Midinfrared Spectroscopy for Analysis and Screening of Liquid Protein Formulations, BioProcess International 4 (2006) 48–55.

[61] M. Byler, H. Susi, Examination of the Secondary Structure of Proteins by Deconvolved FTIR Spectra, Biopolymers, 25 (1986) 469–487.